Engineering subharmonic responses beyond prethermalization via Floquet scar states

Ke Huang and Xiao Li*

Department of Physics, City University of Hong Kong, Kowloon, Hong Kong SAR, China

(Received 4 June 2023; revised 2 January 2024; accepted 25 January 2024; published 13 February 2024)

In this work we propose a scheme to engineer subharmonic responses via scar states in a generalized PXP model. We first show that the generalized PXP model also possesses a band of scar states like the pristine PXP model does. In addition, we reveal that a generalized forward-scattering approximation (FSA) still works for these scar states. We further argue that the FSA subspace exhibits an $SO(3)$ symmetry, which enables an $SO(3)$-FSA approach for the scar states. When such a model is placed under periodic driving, nontrivial Floquet scar states emerge in the quasienergy spectrum. One appealing feature of such Floquet scar states is that they can support subharmonic responses akin to the discrete time crystalline phase. In particular, such subharmonic responses can exist beyond the conventional prethermalization regime, where either large frequencies or large driving amplitudes are required.

DOI: 10.1103/PhysRevB.109.064306

I. INTRODUCTION

Ergodicity in an isolated quantum system is believed to be described by the eigenstate thermalization hypothesis (ETH) [1–4], assuming that eigenstates around the same energy are locally indistinguishable. However, abundant theoretical and experimental evidence suggests that some system breaks the ETH. A well-known example is many-body localization [5–7], which breaks ergodicity in the strong sense: all eigenstates violate the ETH, so all localized initial states retain their memories even after a long period of time evolution. Meanwhile, the ETH can also be weakly broken by embedding rare atypical states in the thermal bulk [8], and only dynamics from particular initial states exhibit nonergodic behavior. Experimentally, the weak ergodicity breaking was first found in the strongly interacting Rydberg atoms [9], in which only quench dynamics from the Z_2 ordered states revive periodically. This phenomenon is theoretically described by a special set of rare eigenstates in the PXP model [10,11]. The periodic revival resembles the scar in the chaotic systems, and thus the rare eigenstates in the PXP model are dubbed quantum many-body scar (QMBS) states.

Beyond isolated systems, people also found nonergodic dynamics in periodically driven or Floquet systems. A prominent example is the discrete time crystal (DTC) stabilized by strong disorders [12–20], in which all initial states exhibit subharmonic responses with respect to the driving period. Meanwhile, there is the so-called prethermal DTC, in which some ergodic initial states may also behave like DTC within an exponentially long time scale [21–24]. Such examples are typically explained within the framework of spontaneous discrete symmetry breaking. Recently, another possibility of ergodicity breaking in Floquet systems emerges, which are known to have Floquet QMBS states by analogy with the isolated systems. A trivial case is that the Hamiltonians at different times share a set of common QMBS states that spontaneously become the Floquet QMBS states. In contrast, several recent works have proposed nontrivial Floquet QMBS states [25–34]. However, such proposals are typically limited by specific parameters or require a high-frequency driving.

In this work, we generalize the PXP model to a three-component model, whose QMBS states can also be approximated by the forward-scattering approximation (FSA) [10,11]. In fact, the generalized PXP model completes the approximate $su(2)/so(3)$ Lie algebra of the pristine PXP model [11,35,36] in the FSA subspace. As a result, the evolution of the system represents the Lie group generated by this Lie algebra. We verify numerically that the Lie group is the $SO(3)$ Lie group instead of the $SU(2)$ Lie group. Facilitated by the group structure, the evolution of a time-dependent generalized PXP model emulates a three-dimensional rotation. Particularly, one can readily engineer a large variety of Floquet systems with different subharmonic revivals (period doubling, tripling, etc.), where the system spontaneously possesses nontrivial Floquet scar states determined by the group structure. Despite the similarity to the prethermal discrete time crystal (DTC), we emphasize that this model is fundamentally different because the generalized PXP model depends on an unbroken continuous symmetry rather than a broken discrete symmetry.

II. THE GENERALIZED PXP MODEL

We start by reviewing the pristine PXP Hamiltonian [10,11]

$$H_x = \sum_r \sigma_r^x \left(\frac{1}{2} + Q_r\right) \prod_{\langle r,r'\rangle} P_{r'}, \tag{1}$$

where $\sigma_r^x, \sigma_r^y, \sigma_r^z$ are Pauli matrices at site r, and $P_r = (\mathbb{1} - \sigma_r^z)/2$ projects into the ground state. For the PXP model, the

*xiao.li@cityu.edu.hk

 ©2024 American Physical Society

Hilbert space is constrained, and no neighboring sites can be simultaneously excited. In addition, Q_r serves as a stabilizer to enhance the weak ergodicity breaking in this model. The forms of Q_r have been proposed for different lattices [35,37], and it is taken as $0.051(\sigma^z_{r+2}+\sigma^z_{r-2})$ in the 1D lattice.

The QMBS states in the PXP model have an equal energy spacing of $\omega_s = 2\pi/T_s$ (where we set $\hbar = 1$ throughout), which is almost independent of the system size. As the pristine PXP Hamiltonian includes only the x component of the spin operators, it is intuitive to introduce the other two components in a 1D bipartite lattice as well, which are given by

$$H_y = \sum_r \mathrm{sgn}(r)\sigma^y_r\left(\frac{1}{2}+Q_r\right)\prod_{\langle r,r'\rangle} P_{r'}, \tag{2}$$

$$H_z = \frac{\omega_s}{2}\sum_r \mathrm{sgn}(r)\sigma^z_r\prod_{\langle r,r'\rangle} P_{r'}. \tag{3}$$

In the above Hamiltonian, the lattice is divided into two sublattices A and B, and we introduce

$$\mathrm{sgn}(r) = \begin{cases} 1, & r\in A,\\ -1, & r\in B.\end{cases} \tag{4}$$

Thus, for an arbitrary unit vector $\vec{n} = (n_x, n_y, n_z)\in\mathbb{R}^3$, we can construct a generalized PXP Hamiltonian as

$$H_{\mathrm{full}} = \vec{n}\cdot\vec{H},\ \text{where}\ \vec{H} = (H_x, H_y, H_z). \tag{5}$$

In what follows, we will study the scar states in this generalized PXP model. For convenience, we will also use the notation that

$$\vec{n} = (\sin\theta\cos\varphi, \sin\theta\sin\varphi, \cos\theta)\equiv(\theta,\varphi). \tag{6}$$

Scar states in the generalized PXP model

We now demonstrate the existence of scar states in H_{full} in Eq. (5). To begin with, note that a bipartite lattice permits two maximally excited states $|M_{\mathrm{A}}\rangle$ and $|M_{\mathrm{B}}\rangle$, defined as the state where all sites on the A or B sublattice are excited, respectively. For a 1D chain with an even number of sites, A and B are the even or the odd sites. Let us denote the subspace spanned by these two states as P_Z. The scars of the system can be identified by their overwhelmingly large projection on P_Z and their significantly small entanglement entropy (EE), defined as $S(|\phi\rangle) = -\mathrm{Tr}\{\rho_{\mathrm{L}}(|\phi\rangle)\ln\rho_{\mathrm{L}}(|\phi\rangle)\}$. In this definition, the system is divided into two subsystems: the left and right half, and $\rho_{\mathrm{L}}(|\phi\rangle) = \mathrm{Tr}_{\mathrm{R}}(|\phi\rangle\langle\phi|)$. These properties are shown in Fig. 1, which implies the existence of scar states in H_{full}.

A hallmark of the pristine PXP model is that the QMBS states can be approximated by the so-called forward-scattering approximation (FSA) [10,11], which considers a specific subspace generated by a pair of ladder operators,

$$H^+ = H_x + iH_y,\quad H^- = H_x - iH_y, \tag{7}$$

and the basis of this FSA subspace is

$$\begin{aligned}|j\rangle &= (H^+)^j|M_{\mathrm{A}}\rangle\times\|(H^+)^j|M_{\mathrm{A}}\rangle\|^{-1},\\ |L-j\rangle &= (H^-)^j|M_{\mathrm{B}}\rangle\times\|(H^-)^j|M_{\mathrm{B}}\rangle\|^{-1},\\ |L/2\rangle &= (H^+|L/2-1\rangle + H^-|L/2+1\rangle)\\ &\quad\times\|H^+|L/2-1\rangle + H^-|L/2+1\rangle\|^{-1},\end{aligned} \tag{8}$$

where $j = 0, 1, \ldots, (L/2)-1$, and L is the number of sites. This idea can also be applied to the generalized PXP model as follows. Consider the FSA Hamiltonian given by $P_F H_{\mathrm{full}} P_F$, where $P_F = \sum_j |j\rangle\langle j|$ projects into the FSA subspace. As in the pristine PXP model, the FSA Hamiltonian here is tridiagonal. In addition, it has nonzero diagonal entries because of H_z. In Fig. 1, we can see clearly that FSA provides an accurate approximation as expected, and the approximation works better for small $|n_z|$.

Moreover, this generalized FSA implies that the scar subspaces of different $\vec{n}$ can be approximated by an $\vec{n}$-independent subspace, the FSA subspace. To quantify this assertion, we first denote $\{|E_j(\vec{n})\rangle\}$ as the set of scars of H_{full}. The projector of the scar subspace is then $P_S(\vec{n}) = \sum_j |E_j(\vec{n})\rangle\langle E_j(\vec{n})|$. Further, we introduce the normalized Frobenius norm,

$$\|X\| \equiv [\mathrm{Tr}(X^\dagger X)/(L+1)]^{1/2}. \tag{9}$$

Under this convention, we have $\|P_S(\vec{n})\| = \|P_F\| = 1$, and the difference between the FSA subspace and the scar subspace can be estimated by $\|P_S(\vec{n}) - P_F\|$. Additionally, $\|P_S(\vec{n}) - P_F\|$ is φ-independent because of $[H_z, P_F] = 0$ and the exact z-axis symmetry

$$[R_z(\alpha)\vec{n}]\cdot\vec{H} = U^\dagger(\vec{n}\cdot\vec{H})U, \tag{10}$$

where $U = e^{-i\alpha H_z/\omega_s}$ and $R_z(\alpha)$ is the rotation around the z axis for an angle α. As a result, we will only consider $\vec{n}$ with $\varphi = 0$ (or $n_y = 0$) henceforth without loss of generality. Figure 2 shows that the FSA subspace is indeed a good approximation of the scar subspace for small $|n_z|$. Though the approximation is not as good for large $|n_z|$ as for small $|n_z|$, the error is on the same order of that in the original PXP model studied in Ref. [10]. Therefore, we have demonstrated that the FSA subspace is approximately an invariant subspace for all H_{full}.

More interestingly, H_{full} possesses an approximate $su(2)$ Lie algebra on the FSA subspace [11,35,36], i.e.,

$$[P_F H_a P_F, P_F H_b P_F] \approx i\varepsilon_{abc}\,\omega_s P_F H_c P_F, \tag{11}$$

where $a, b, c = x, y, z$. Hence, what remains to resolve is which symmetry group [$SO(3)$ or $SU(2)$] can best describe the FSA subspace. The first hint is that the dimension of the FSA subspace is always odd because we consider *bipartite lattices* only, implying that it may be a representation of $SO(3)$. Furthermore, one can show that for arbitrary unit vectors $\vec{n}_1, \vec{n}_2$ and rotation angles $\omega_s T_1, \omega_s T_2$, there exist $\vec{n}_3$ and T_3 satisfying

$$R(\vec{n}_2, \omega_s T_2)R(\vec{n}_1, \omega_s T_1) = R(\vec{n}_3, \omega_s T_3), \tag{12}$$

$$P_F e^{-iT_2\vec{n}_2\cdot\vec{H}} e^{-iT_1\vec{n}_1\cdot\vec{H}} P_F \approx P_F e^{-iT_3\vec{n}_3\cdot\vec{H}} P_F, \tag{13}$$

where $R(\vec{n}, \alpha)$ represents the rotation around $\vec{n}$ for an angle α. As a result, the approximate symmetry of the FSA subspace is $SO(3)$ instead of $SU(2)$ in this bipartite lattice. We will see that this approximate $SO(3)$ symmetry of the FSA subspace is crucial for our design of the subharmonic response when the generalized PXP model is placed under periodic driving.

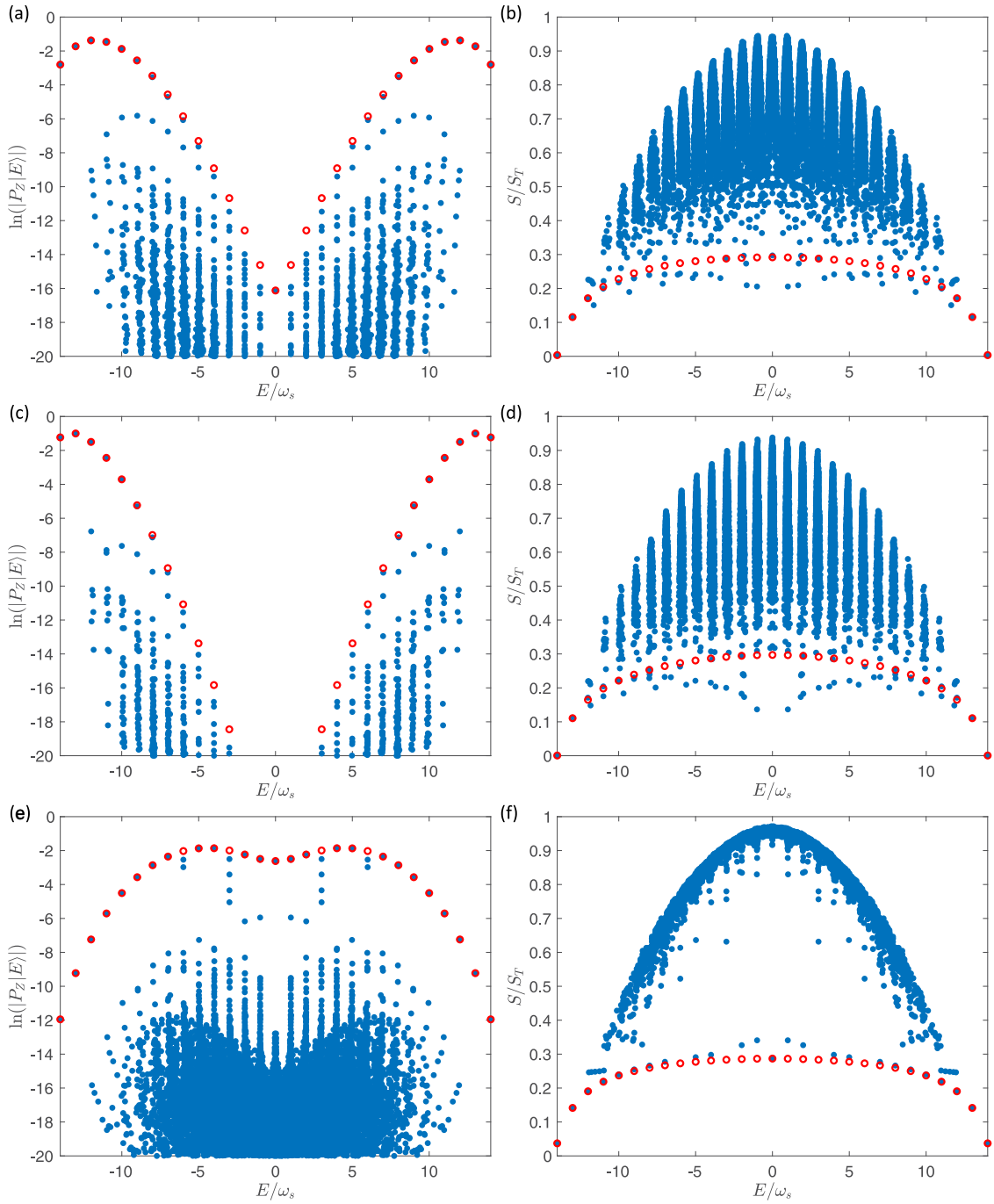

FIG. 1. The left panel plots the projection, and the right panel plots the half-chain EE in an $L = 28$ chain. Here we take $\vec{n} = (\pi/5, 0)$ (large $|n_z|$) in (a) and (b), $\vec{n} = (\pi/5 + 2\pi/3, 0)$ (large $|n_z|$) in (c) and (d), and $\vec{n} = (2\pi/5, \pi/2)$ (small $|n_z|$) in (e) and (f). The EE in the thermal limit is $S_T = \ln(F_{L/2+2}) - 1/2$ for 1D chains, where F_n is the nth Fibonacci number. Here, the blue dots are obtained by diagonalizing the exact Hamiltonian, and the red circles are the FSA.

III. THE GENERALIZED PXP MODEL UNDER PERIODIC DRIVING

In the pristine PXP model, the presence of QMBS states with equal energy spacing results in weak ergodicity breaking. This phenomenon can also be observed in the Floquet PXP model, as we now show. Specifically, we study the dynamics from the initial state $|\mathbb{Z}_2\rangle = |M_{\mathrm{A}}\rangle$ [38], and introduce a time-periodic Hamiltonian $H(t)$ with a period of $T = T_1 + T_2$,

$$H(t) = \begin{cases} \vec{n}_1 \cdot \vec{H}, & 0 < t < T_1, \\ \vec{n}_2 \cdot \vec{H}, & T_1 < t < T_1 + T_2, \end{cases} \tag{14}$$

where $\vec{n}_1, \vec{n}_2$ are unit vectors in $\mathbb{R}^3$. As the FSA subspace approximates the true scar subspace for all $\vec{n}$, the FSA

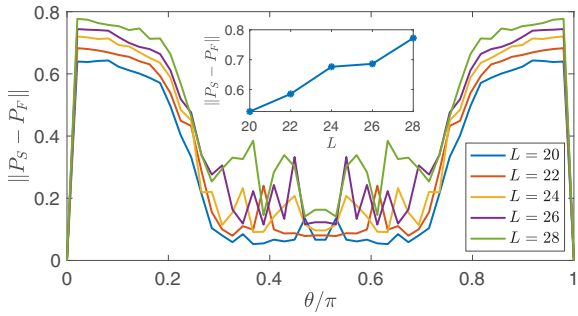

FIG. 2. A plot of $\|P_S - P_F\|$ as a function of θ. The inset calculates the PXP model in Ref. [10], which has no stabilizer Q_r. We thus see that the FSA subspace provides a good approximation for the scar subspace.

Hamiltonian $P_F H(t) P_F$ applies to the dynamics of $|\mathbb{Z}_2\rangle$ in the Floquet system as well. In particular, under FSA, the time evolution operator is approximated by

$$U(t) \approx U_{\text{FSA}}(t) \equiv \mathcal{T} \exp\left[-i \int_0^t P_F H(s) P_F \, \mathrm{d}s\right], \tag{15}$$

where $\mathcal{T}$ is the time ordering operator.

From the $SO(3)$ symmetry perspective in Eq. (13), we know that $H(t)$ executes a rotation $R(t)$ in $\mathbb{R}^3$. Knowing that $R(t)$ can be uniquely expressed as $R(t) = R(\vec{n}_3(t), \omega_s T_3(t))$, where $\vec{n}_3(t)$ and $T_3(t)$ are continuous functions, we introduce an $SO(3)$-FSA approximation for $U(t)$, given by

$$U(t) \approx U_{SO(3)\text{-FSA}}(t) \equiv e^{-iT_3(t)\vec{n}_3(t)\cdot P_F \vec{H} P_F}. \tag{16}$$

Given that a revival is equivalent to $R(t)$ becoming the identity, we can engineer the revival period to be *any* integer multiple of the driving period.

For definiteness, here we demonstrate a period tripling case and leave the period quadrupling case to the appendices. As the evolution emulates a 3-dimensional rotation, there are infinite ways to engineer a period-tripling response. For instance, $\vec{n}_1 = (\theta, 0)$, $\vec{n}_1 = (\theta + 2\pi/3, 0)$ together with $T_1 = T_2 = T_s/2$ give a period-tripling response for any θ, and particularly, we take $\theta = -\pi/5$. We start by showing that $|\mathbb{Z}_2(t)\rangle$ still almost stays within the FSA subspace even for $t = 20T_s$, as shown in Fig. 3(a). Then, the fidelity $F(t) = |\langle \mathbb{Z}_2 | \mathbb{Z}_2(t)\rangle|^2$ calculated through FSA and $SO(3)$-FSA is compared with that obtained by diagonalizing the exact Floquet operator. We find that both $SO(3)$-FSA and FSA offer a good approximation after a long-time evolution (up to $t \sim 20T_s$), as shown in Fig. 3(b). This verifies our assertion that the FSA subspace has an approximate $SO(3)$ symmetry.

We also study the error of the two approximations by evaluating the norm between the approximated states and the exact results, which are shown in Fig. 3(c). We find that the FSA generally fits the exact results fairly well. In contrast, the difference between the $SO(3)$-FSA approximation and the exact results continues to increase. The error of $SO(3)$-FSA comes from both the leakage of the FSA subspace and the imperfection of the $SO(3)$ structure, and causes the decay of the fidelity at the revival. Particularly, we observe that the early decay manifests the following empirical scaling relation

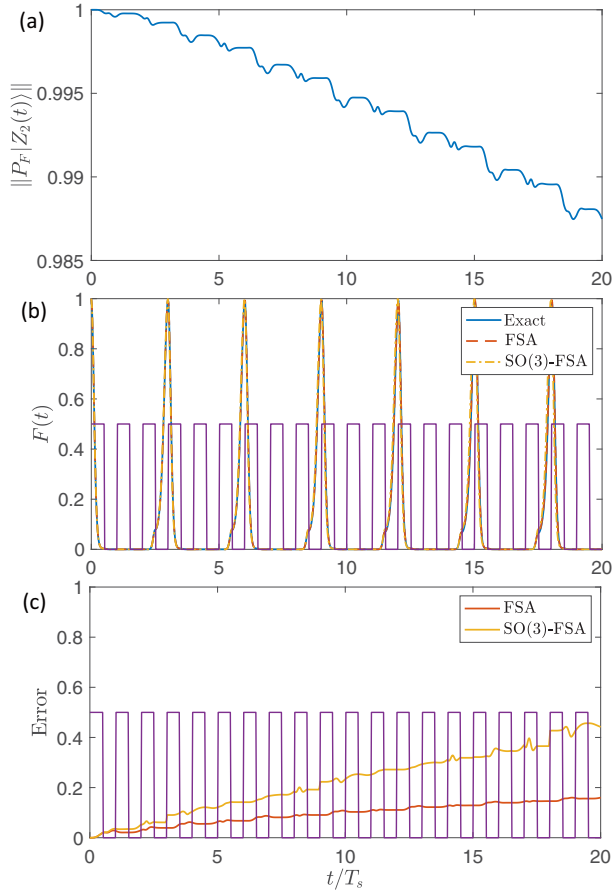

FIG. 3. Panels (a)–(c) plot the projection in the FSA subspace, the fidelity, and the accuracy of two FSAs, respectively. Here we use an $L = 28$ chain ($T_s = 9.8987$), with parameters $\vec{n}_1 = (-\pi/5, 0)$, $\vec{n}_2 = (-\pi/5 + 2\pi/3, 0)$, $T_1 = T_s/2$, and $T_2 = T_s/2$. The purple lines in (b) and (c) equal 1/2 when $\vec{n}_1 \cdot \vec{H}$ is turned on, and equals zero otherwise.

as shown in Fig. 4,

$$[1 - F(t)]/L \approx \alpha (t/T_s)^{\gamma}, \tag{17}$$

where $\alpha = 5.16 \times 10^{-5}$ and $\gamma = 1.68$ are the fitting parameters. Hence, we estimate that the fidelity remains greater than 0.9 at $t = 21T_s$ in the system of $L = 100$, which is typically the experimental size.

The observed periodic revivals suggest the existence of Floquet QMBS states in the system described by Eq (14). In

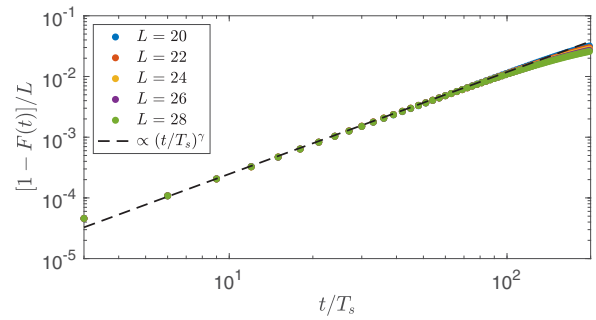

FIG. 4. Finite-size scaling of the fidelity. The parameters are given in Fig. 3.

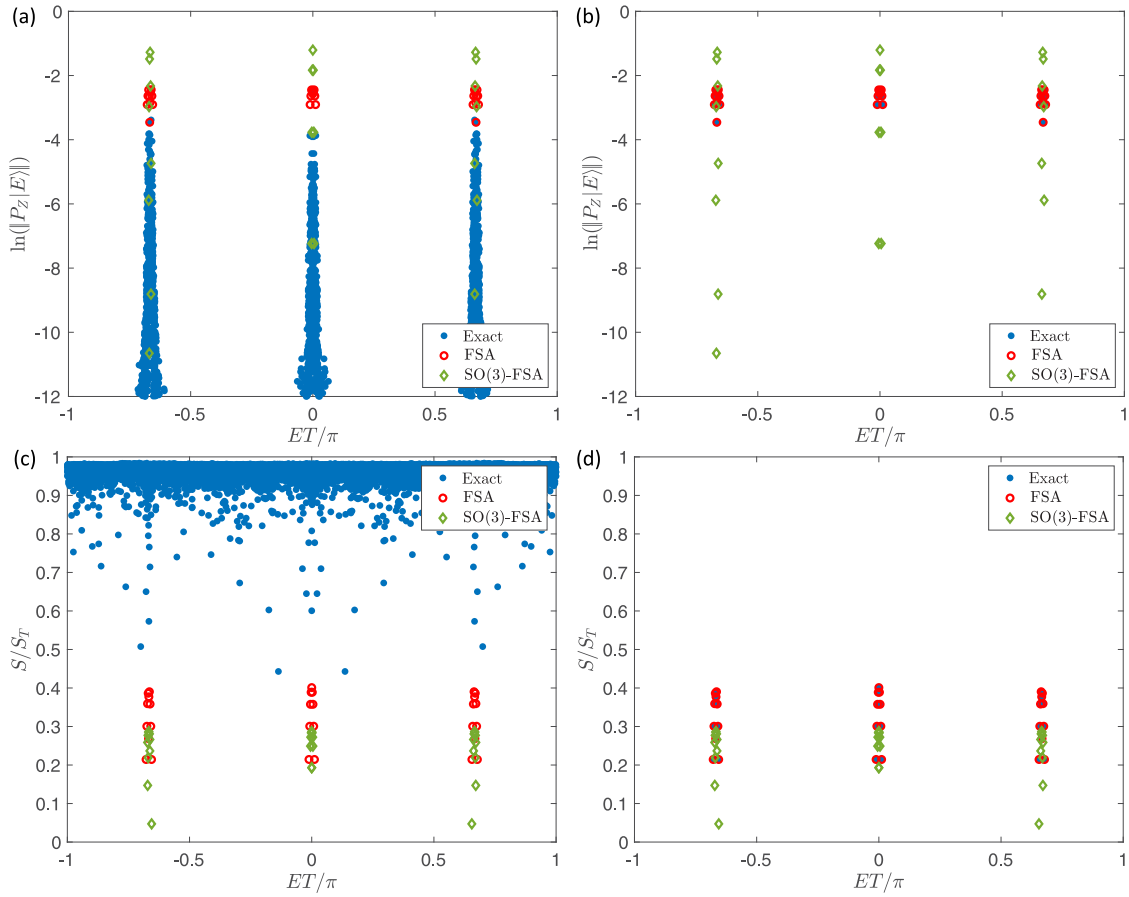

FIG. 5. Here we show the projection and the EE of the eigenstates derived from three different approaches. The exact results in the left and the right panel represent the eigenstates of $U(T)$ and $P_F U(T) P_F$, respectively. The parameters are given in Fig. 3.

particular, they are the eigenstates of a Floquet Hamiltonian $\mathcal{H}_{\rm F}$, defined by way of

$$e^{-iT\mathcal{H}_{\rm F}} \equiv U(T) = e^{-iT_2\vec{n}_2\cdot\vec{H}} e^{-iT_1\vec{n}_1\cdot\vec{H}}. \tag{18}$$

What is more, the Floquet QMBS states cannot be trivial because $\vec{n}_1\cdot\vec{H}$ and $\vec{n}_2\cdot\vec{H}$ generally share no common eigenstates. Notwithstanding, as the FSA subspace is approximately invariant, Eq. (15) suggests that $\mathcal{H}_{\rm F}$ is approximated by the Floquet Hamiltonian $\mathcal{H}_{\rm F}^{\rm FSA}$ defined by $e^{-iT\mathcal{H}_{\rm F}^{\rm FSA}} \equiv U_{\rm FSA}(T)$, which is expected to capture the QMBS states. Meanwhile, Eq. (16) implies that under $SO(3)$-FSA, $\mathcal{H}_{\rm F}$ is approximated by

$$P_F\mathcal{H}_{\rm F}P_F \approx \mathcal{H}_{\rm F}^{SO(3)\text{-FSA}} \equiv \frac{T_3(T)}{T} P_F[\vec{n}_3(T)\cdot\vec{H}]P_F. \tag{19}$$

The importance of this approximation is to explain the periodic revivals in our model, as not all QMBS states support periodic revivals.

In Fig. 5, we study the eigenstates of $U(T)$ and $P_F U(T) P_F$ (exact) by exact diagonalization and compare them with the results obtained by FSA and $SO(3)$-FSA. Noting the equivalence between $ET = \pm\pi$ in the quasienergy spectrum, we find in Fig. 5(a) that the eigenstates of $U(T)$ form a tower structure and that they concentrate within a narrow energy window around the quasienergies given by the FSA and the $SO(3)$-FSA approaches. However, neither approximations predicts the projection $\ln(\|P_Z|E\rangle\|)$ very well. The reason is that the model does not have actual eigenstates serving as the QMBS states. Instead, the system possesses several towers of eigenstates, which can be regarded as bands of degenerate states within a small timescale. Therefore, before full thermalization, the superposition of each tower of states plays the role of QMBS states. However, we emphasize that because of the extremely small bandwidth, the relaxation time here is still rather long with respect to the typical timescale T_s, as shown in Fig. 3(a). Furthermore, Fig. 3(a) suggests that the short-time evolution happens essentially within the FSA subspace. Therefore, the superposition should be described by the eigenstates of $P_F U(T) P_F$ calculated in Fig. 5(b). For the subharmonic responses in our model, we observe that the eigenstates of $P_F U(T) P_F$ can be perfectly approximated by the FSA method, whereas the $SO(3)$-FSA only gives the correct energy but not the projection. The reason is that the spectrum, in this case, is highly degenerate. Consequently, the imperfection of the symmetry on the FSA subspace serves as a small perturbation and creates a significant correction to the eigenstates (but only a small correction to the spectrum). This is in contrast to the general case in the appendices, where the spectrum is nondegenerate, and thus both FSA and $SO(3)$-FSA work well for the projection.

Finally, we investigate the EE of the Floquet eigenstates in Fig. 5(c). We find that the eigenstates of $U(T)$ are all highly entangled. In contrast, as shown in Fig. 5(d), the short-time evolution is dominated by their low-entangled superpositions.

What is more, the FSA approach works perfectly for the EE, and the $SO(3)$-FSA also provides a good approximation. Besides, we have studied a more general case in the appendices. We show that it also possesses the nontrivial Floquet QMBS and find that the two approximations [FSA and $SO(3)$-FSA] are even better in that case because there is generally no degeneracy unless deliberately designed.

IV. DISCUSSION AND CONCLUSION

In this work, we study a generalized PXP model whose QMBS states are well described by an FSA subspace that is universal for all choices of $\vec{n}$. Hence, the FSA subspace is approximately an invariant subspace of the generalized PXP model, which carries an approximate $SO(3)$ symmetry. As a result, the evolution in the FSA subspace of a time-dependent system can be solved by a pair of time-dependent rotation axes and angles. Utilizing this property, we have much freedom to design the system, and particularly, we engineer a Floquet system with period-tripling revivals in the main text. Moreover, the group structure also reveals that the Floquet Hamiltonian is actually captured by another generalized PXP model, which carries nontrivial Floquet QMBS states.

Despite the resemblance to the prethermal DTC in the literature [21–23,33], there are important differences between our protocol and the earlier work. For example, the subharmonic response here arises from the continuous symmetry $SO(3)$, while prethermal DTCs spontaneously break a discrete symmetry. In particular, the subharmonic response in our model arises from a carefully engineered orbit in the $SO(3)$ subspace. Deviations from this protocol will introduce errors in the subharmonic response. This work also shows the probability of QMBS states in the nearly degenerate systems in which QMBS states are not exact eigenstates but their superpositions.

Note added. We recently became aware of an independent work exploring a similar idea in a different setup [39].

ACKNOWLEDGMENTS

This work is supported by the Research Grants Council of Hong Kong (Grants No. CityU 21304720, No. CityU 11300421, No. CityU 11304823, and No. C7012-21G) and City University of Hong Kong (Projects No. 9610428 and No. 7005938). K.H. is also supported by the Hong Kong PhD Fellowship Scheme.

APPENDIX A: ENGINEERING GENERIC FLOQUET EVOLUTIONS

In this section, we study a more general case for the Floquet Hamiltonian in Eq. (14). We first discuss a period quadrupling case, which is shown in Figs. 6(a) and 6(b) with parameters $\vec{n}_1 = (\pi/5, 0)$, $\vec{n}_2 = (\pi/5 + 3\pi/4, 0)$, $T_1 = T_s/2$, and $T_2 = T_s/2$. Similar to the period-tripling case, the dynamics can

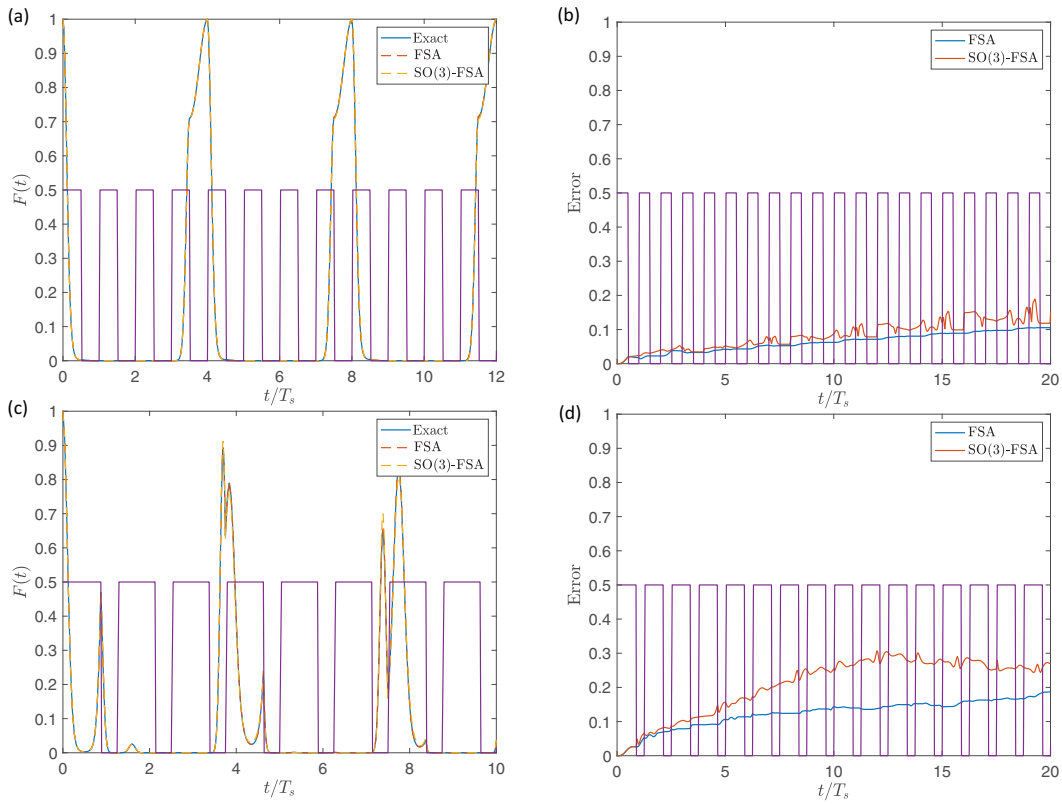

FIG. 6. Panels (a) and (b) show the fidelity and the accuracy, respectively, in an $L = 28$ chain ($T_s = 9.8987$), with parameters $\vec{n}_1 = (\pi/5, 0)$, $\vec{n}_2 = (\pi/5 + 3\pi/4, 0)$, $T_1 = T_s/2$, and $T_2 = T_s/2$. Panels (c) and (d) show the fidelity and the accuracy, respectively, in an $L = 28$ chain ($T_s = 9.8987$), with parameters $\vec{n}_1 = (\pi/5, 0)$, $\vec{n}_2 = (2\pi/5, \pi/2)$, $T_1 = 7T_s/8$, $T_2 = 3T_s/8$. The purple lines in the four panels equal 1/2 when $\vec{n}_1 \cdot \vec{H}$ is turned on and 0 otherwise.

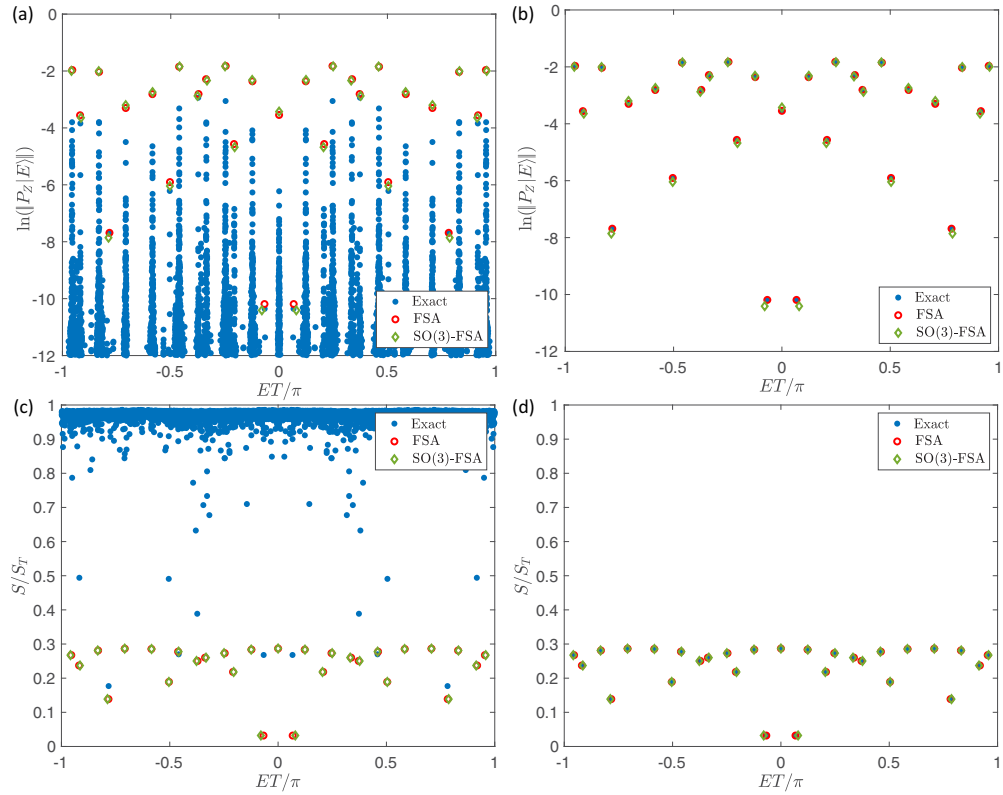

FIG. 7. The projection and the EE of the eigenstates derived from three different approaches. The exact results in the left and the right panel represent the eigenstates of F and $P_F F P_F$, respectively. The parameters used in this figure are identical to those in Fig. 6.

be accurately captured by the $SO(3)$ structure in the FSA subspace.

A more generic scenario of the $SO(3)$ structure can also be found in systems without subharmonic responses. Particularly, we take $\vec{n}_1 = (\pi/5, 0)$, $n_2 = (2\pi/5, \pi/2)$, and $T_1 = 7T_s/8$, $T_2 = 3T_s/8$. Note that the properties of $\vec{n}_{1,2} \cdot \vec{H}$ have been studied in Fig. 1. We first study the dynamics of $|\mathbb{Z}_2\rangle$. In Fig. 6(c), two approximations fit the exact results excellently, and Fig. 6(d) even suggests that the $SO(3)$-FSA approach is better here than the case in the main text. Another intriguing phenomenon here is that as the system is not carefully designed, there is never perfect revival; i.e., the corresponding 3D rotation $R(t)$ never becomes the identity.

In addition, we also compute the Floquet eigenstates of this system, which are shown in Fig. 7. This generic system manifests similar features to the case in the main text; i.e., highly entangled eigenstates form tower structures whose superposition serves as the scar states. However, the most significant difference here is that the $SO(3)$-FSA approach is almost as accurate as the FSA approach, indicating the universal applicability of the $SO(3)$-FSA approach.

APPENDIX B: THE FATE OF IMPERFECT REVIVALS

In the previous section, we demonstrate that the revival is generally imperfect without deliberate design. Hence, a natural question is whether these imperfect revivals survive in the thermodynamic limit. For a perfect $SO(3)$ representation, the question is equivalent to proving the following limit,

$$\lim_{j\to\infty} |\langle j, j, \vec{z}|U_j(R)|j, j, \vec{z}\rangle| = 0, \tag{B1}$$

where $|l, m, \vec{n}\rangle$ is the eigenstate of $\vec{n} \cdot J$ with $\vec{J}^2|l, m, \vec{n}\rangle = l(l+1)|l, m, \vec{n}\rangle$ and $\vec{n} \cdot J|l, m, \vec{n}\rangle = m|l, m, \vec{n}\rangle$. Here, $U_l(R)$ is the corresponding $(2l+1)$-dimensional irreducible representation of $R \in SO(3)$.

To start, we first prove the following lemma: For all l, m, and two unit vectors $\vec{n}, \vec{n}'$, the following inequality holds,

$$|\langle l, m, \vec{n}|l, m, \vec{n}'\rangle| \leqslant \left[1 + \frac{2m^2 \tan^2(\theta/2)}{l(l+1) - m^2}\right]^{-1/2}, \tag{B2}$$

where θ is the angle between $\vec{n}$ and $\vec{n}'$. To show this, first note that the inequality holds trivially if $\vec{n} = \pm\vec{n}'$. Hence, we only consider that $\vec{n}$ and $\vec{n}'$ are not parallel, or equivalently $\sin\theta \neq 0$. Without loss of generality, we set $\vec{n} = \vec{z}$. Further, because

$$\begin{aligned} |\langle l, m, \vec{n}|, m, \vec{n}'\rangle| &= |e^{im\phi}\langle l, m, \vec{n}|, m, \vec{n}'\rangle| \\ &= \left|\langle l, m, \vec{n}|e^{-i\phi J_{\vec{l}}}|l, m, \vec{n}'\rangle\right| \\ &= |\langle l, m, \vec{n}|l, m, R_z(\phi)\vec{n}'\rangle|, \end{aligned} \tag{B3}$$

where we have we set $\vec{n}'$ in the x-z plane, with $\vec{n}' = \cos\theta\vec{z} + \sin\theta\vec{x}$.

Now let $|\psi\rangle = \sum_k \psi_k|l, k\rangle$ be the eigenvalue of $\vec{n}' \cdot \vec{J}_l$ with eigenvalue m, and then we have

$$|\langle l, m, \vec{n}|l, m, \vec{n}'\rangle| = \frac{|\psi_m|}{\||\psi\rangle\|}. \tag{B4}$$

We suppose that $\psi_m \neq 0$; otherwise the lemma is proved. Therefore, we can set $\psi_m = 1$, and

$$\begin{aligned} m &= \langle l, m|\vec{n}' \cdot \vec{J}_l|\psi\rangle \\ &= m\cos\theta + \frac{\sin\theta}{2}\psi_{m+1}\sqrt{l(l+1)-m(m-1)} \\ &\quad + \frac{\sin\theta}{2}\psi_{m-1}\sqrt{l(l+1)-m(m+1)}, \end{aligned} \tag{B5}$$

which can be rewritten as

$$\begin{aligned} 2m\tan(\theta/2) &= \psi_{m+1}\sqrt{l(l+1)-m(m+1)} \\ &\quad + \psi_{m-1}\sqrt{l(l+1)-m(m-1)}. \end{aligned} \tag{B6}$$

From the Cauchy inequality, we have

$$\tan^2(\theta/2) \leqslant \frac{l(l+1)-m^2}{2m^2}(|\psi_{m+1}|^2 + |\psi_{m-1}|^2), \tag{B7}$$

so we can further derive

$$\begin{aligned} \||\psi\rangle\|^2 &\geqslant (|\psi_{m+1}|^2 + |\psi_m|^2 + |\psi_{m-1}|^2) \geqslant 1 \\ &\quad + \frac{2m^2\tan^2(\theta/2)}{l(l+1)-m^2}. \end{aligned} \tag{B8}$$

Hence we have

$$\begin{aligned} |\langle l, m, \vec{n}|l, m, \vec{n}'\rangle| &= |\psi_m|/\||\psi\rangle\| \\ &\leqslant \left[1 + \frac{2m^2\tan^2(\theta/2)}{l(l+1)-m^2}\right]^{-1/2}, \end{aligned} \tag{B9}$$

which completes the proof of the lemma.

According to the lemma, it is straightforward to derive the following theorem: For an arbitrary non-negative integer k, a rotation R, and a unit vector $\vec{n}$, we have

$$\lim_{l\to\infty} |\langle l, l-k, \vec{n}|U_l(R)|l, l-k, \vec{n}\rangle| = \delta_{\vec{n},R\vec{n}}, \tag{B10}$$

where $\delta_{\vec{n},\vec{n}} = 1$ and $\delta_{\vec{n},\vec{n}'} = 0$ if $\vec{n} \neq \vec{n}'$. First, noticing that $|\langle l, l-k, \vec{n}|U_l(R)|l, l-k, \vec{n}\rangle| = |\langle l, l-k, \vec{n}|l, l-k, R\vec{n}\rangle|$, according to the lemma, we have

$$|\langle l, l-k, \vec{n}|U_l(R)|l, l-k, \vec{n}\rangle| \leqslant \left[1 + \frac{2m^2\tan^2(\theta/2)}{l(l+1)-m^2}\right]^{-\frac{1}{2}}.$$

If $\vec{n} = R\vec{n}$, then $|\langle l, l-k, \vec{n}|U_l(R)|l, l-k, \vec{n}\rangle| = 1$ and the limit equals 1. If $\vec{n} \neq R\vec{n}$, we know that

$$\lim_{l\to\infty}\left[1 + \frac{2(l-k)^2\tan^2(\theta/2)}{l(l+1)-(l-k)^2}\right]^{-1/2} = 0, \tag{B11}$$

and therefore, we have

$$\lim_{l\to\infty} |\langle l, l-k, \vec{n}|U_l(R)|l, l-k, \vec{n}\rangle| = 0. \tag{B12}$$

In conclusion, for a perfect $SO(3)$ structure, all imperfect revivals vanish in the thermodynamic limit, whereas the perfect revival is always perfect. Hence, the imperfect revival will decay with system size even faster in the PXP model because of both the imperfection of $SO(3)$ and the leakage of the FSA subspace.

[1] J. M. Deutsch, Phys. Rev. A **43**, 2046 (1991).
[2] M. Srednicki, Phys. Rev. E **50**, 888 (1994).
[3] M. Rigol, V. Dunjko, and M. Olshanii, Nature (London) **452**, 854 (2008).
[4] T. Mori, T. N. Ikeda, E. Kaminishi, and M. Ueda, J. Phys. B: At., Mol. Opt. Phys. **51**, 112001 (2018).
[5] R. Nandkishore and D. A. Huse, Annu. Rev. Condens. Matter Phys. **6**, 15 (2015).
[6] E. Altman and R. Vosk, Annu. Rev. Condens. Matter Phys. **6**, 383 (2015).
[7] D. A. Abanin, E. Altman, I. Bloch, and M. Serbyn, Rev. Mod. Phys. **91**, 021001 (2019).
[8] N. Shiraishi and T. Mori, Phys. Rev. Lett. **119**, 030601 (2017).
[9] H. Bernien, S. Schwartz, A. Keesling, H. Levine, A. Omran, H. Pichler, S. Choi, A. S. Zibrov, M. Endres, M. Greiner, V. Vuletić, and M. D. Lukin, Nature (London) **551**, 579 (2017).
[10] C. J. Turner, A. A. Michailidis, D. A. Abanin, M. Serbyn, and Z. Papić, Nat. Phys. **14**, 745 (2018).
[11] C. J. Turner, A. A. Michailidis, D. A. Abanin, M. Serbyn, and Z. Papić, Phys. Rev. B **98**, 155134 (2018).
[12] V. Khemani, A. Lazarides, R. Moessner, and S. L. Sondhi, Phys. Rev. Lett. **116**, 250401 (2016).
[13] D. V. Else, B. Bauer, and C. Nayak, Phys. Rev. Lett. **117**, 090402 (2016).
[14] N. Y. Yao, A. C. Potter, I.-D. Potirniche, and A. Vishwanath, Phys. Rev. Lett. **118**, 030401 (2017).
[15] J. Zhang, P. W. Hess, A. Kyprianidis, P. Becker, A. Lee, J. Smith, G. Pagano, I.-D. Potirniche, A. C. Potter, A. Vishwanath, N. Y. Yao, and C. Monroe, Nature (London) **543**, 217 (2017).
[16] S. Choi, J. Choi, R. Landig, G. Kucsko, H. Zhou, J. Isoya, F. Jelezko, S. Onoda, H. Sumiya, V. Khemani, C. von Keyserlingk, N. Y. Yao, E. Demler, and M. D. Lukin, Nature (London) **543**, 221 (2017).
[17] J. Randall, C. E. Bradley, F. V. van der Gronden, A. Galicia, M. H. Abobeih, M. Markham, D. J. Twitchen, F. Machado, N. Y. Yao, and T. H. Taminiau, Science **374**, 1474 (2021).
[18] X. Mi *et al.*, Nature (London) **601**, 531 (2022).
[19] P. Frey and S. Rachel, Sci. Adv. **8**, eabm7652 (2022).
[20] H. Xu, J. Zhang, J. Han, Z. Li, G. Xue, W. Liu, Y. Jin, and H. Yu, arXiv:2108.00942.
[21] D. Abanin, W. De Roeck, W. W. Ho, and F. Huveneers, Commun. Math. Phys. **354**, 809 (2017).
[22] D. V. Else, B. Bauer, and C. Nayak, Phys. Rev. X **7**, 011026 (2017).
[23] N. Maskara, A. A. Michailidis, W. W. Ho, D. Bluvstein, S. Choi, M. D. Lukin, and M. Serbyn, Phys. Rev. Lett. **127**, 090602 (2021).
[24] A. Kyprianidis, F. Machado, W. Morong, P. Becker, K. S. Collins, D. V. Else, L. Feng, P. W. Hess, C. Nayak, G. Pagano, N. Y. Yao, and C. Monroe, Science **372**, 1192 (2021).
[25] S. Pai and M. Pretko, Phys. Rev. Lett. **123**, 136401 (2019).

[26] B. Mukherjee, S. Nandy, A. Sen, D. Sen, and K. Sengupta, Phys. Rev. B **101**, 245107 (2020).
[27] B. Mukherjee, A. Sen, D. Sen, and K. Sengupta, Phys. Rev. B **102**, 075123 (2020).
[28] K. Mizuta, K. Takasan, and N. Kawakami, Phys. Rev. Res. **2**, 033284 (2020).
[29] H. Yarloo, A. Emami Kopaei, and A. Langari, Phys. Rev. B **102**, 224309 (2020).
[30] S. Sugiura, T. Kuwahara, and K. Saito, Phys. Rev. Res. **3**, L012010 (2021).
[31] P.-G. Rozon, M. J. Gullans, and K. Agarwal, Phys. Rev. B **106**, 184304 (2022).
[32] A. Haldar, D. Sen, R. Moessner, and A. Das, Phys. Rev. X **11**, 021008 (2021).
[33] B. Huang, T.-H. Leung, D. M. Stamper-Kurn, and W. V. Liu, Phys. Rev. Lett. **129**, 133001 (2022).
[34] A. Hudomal, J.-Y. Desaules, B. Mukherjee, G.-X. Su, J. C. Halimeh, and Z. Papić, Phys. Rev. B **106**, 104302 (2022).
[35] S. Choi, C. J. Turner, H. Pichler, W. W. Ho, A. A. Michailidis, Z. Papić, M. Serbyn, M. D. Lukin, and D. A. Abanin, Phys. Rev. Lett. **122**, 220603 (2019).
[36] I. Mondragon-Shem, M. G. Vavilov, and I. Martin, PRX Quantum **2**, 030349 (2021).
[37] A. A. Michailidis, C. J. Turner, Z. Papić, D. A. Abanin, and M. Serbyn, Phys. Rev. Res. **2**, 022065(R) (2020).
[38] However, we note that the physics we discuss applies to all initial states in the scar subspace.
[39] W. Deng and Z.-C. Yang, Phys. Rev. B **108**, 205129 (2023).